Phys. Status Solidi A **211,** No. 10, 2209–2222 (2014) / **DOI** 10.1002/pssa.201431414

Part of Topical Section
Recent Advances on Diamond Surfaces and Devices

physica status solidi a
www.pss-a.com
applications and materials science

Feature Article

Photoelectron emission from lithiated diamond

Kane M. O'Donnell[*,1], Tomas L. Martin[2], Mark T. Edmonds[3], Anton Tadich[4], Lars Thomsen[4], Jürgen Ristein[5], Christopher I. Pakes[6], Neil A. Fox[7], and Lothar Ley[5]

[1] Department of Imaging and Applied Physics, Curtin University, Kent St, Bentley 6102, WA, Australia
[2] Department of Materials, University of Oxford, Parks Road, Oxford, OX1 3PH, United Kingdom
[3] School of Physics, Monash University, Wellington Road, Clayton 3168, VIC, Australia
[4] Australian Synchrotron, 800 Blackburn Road, Clayton 3168, VIC, Australia
[5] Institut für Technische Physik, Universität Erlangen, Staudtstrasse, Erlangen 91058, Germany
[6] Department of Physics, La Trobe University, Bundoora 3086, VIC, Australia
[7] H. H. Wills Physics Laboratory, University of Bristol, Tyndall Avenue, Clifton BS8 1FD, United Kingdom

Received 5 June 2014, revised 2 July 2014, accepted 8 July 2014
Published online 19 August 2014

Keywords diamond, electron affinity, electron emission, lithium, negative, photoemission

[*] Corresponding author: e-mail kane.odonnell@curtin.edu.au, Phone: +61 8 9266 1381, Fax: +61 8 9266 2377

This paper reviews electron emission from negative electron affinity (NEA) diamond and gives account of the recent developments in alternatives to hydrogen-termination for producing NEA diamond surfaces, particularly using lithium on oxygen-terminated diamond. We discuss the background and motivation for using alkali metals and present both experimental and computational results that cover structure, electronic properties, photoemission, and total photoyield. Secondary yield enhancement of over 200 × is demonstrated over a reference surface with positive electron affinity.

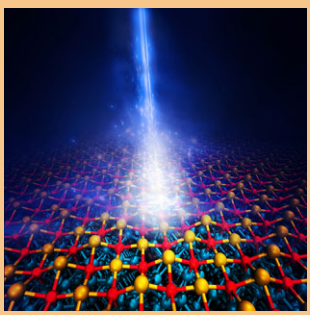

1 Introduction Electron emission is a venerable and well-established subject of materials physics, yet it remains a fruitful and fascinating area of research. New materials and fabrication processes mean that every year many articles communicate advances in the field. For electron emission, diamond is possibly the most important and promising material as it is the only known semiconductor to possess true negative electron affinity (NEA), a state where the conduction band minimum lies above the vacuum level. A material with NEA permits barrier-free electron emission for an electron in the conduction band. Furthermore, electrons excited into the conduction band thermalize rapidly to the conduction band minimum (CBM) and can then travel distances much further than the usual mean free path. Consequently, the secondary electron yield for a NEA material is vastly improved relative to materials with positive electron affinity (PEA) because electrons excited deep in the solid are able to reach the surface and escape. This makes NEA materials ideal for any application requiring high electron yield: photocathodes [1–3], amplifier cathodes [4], vacuum electronic devices [5], thermionic converter cathodes [6] and novel photochemistry [7].

Diamond was first identified as having a negative electron affinity by Himpsel in 1979 on a natural, boron-doped (111)-oriented crystal [8]. The surface was most likely hydrogen-terminated as is typical for natural polished diamonds [9]. Subsequently hydrogen-terminated diamond of both (111) and (100) orientations were investigated by numerous groups and it was determined by total photoyield spectroscopy (TPYS) that both these diamond surfaces exhibit NEA [10–12]. Hydrogen-terminated diamond has subsequently become the standard surface for NEA studies,

with the (100) orientation more common due to the widespread availability of both (100)-oriented single crystals and polycrystalline surfaces with a dominant (100) orientation resulting from the use of Si(100) wafers as the growth substrate.

There has been a steady interest in alternatives to hydrogen termination to generate NEA diamond since the early 90s. These developments are reviewed in the next section, however until the last few years no viable alternative to hydrogen has been developed due to the inherent convenience of the hydrogen-terminated surface for traditional surface science studies. Recently, it has been recognized that alternatives would be useful for applications involving poor vacuum or occasional air exposure. Hydrogen-terminated diamond is not suited to such applications for two reasons. First, water adsorption on hydrogen-terminated diamond leads to charge transfer and concomitant upwards band-bending [13, 14] that neutralizes the advantages of NEA for electron emission; thus the highly interesting and useful phenomenon of diamond surface conductivity is in fact a drawback for electron emission devices.

The second reason hydrogen-terminated diamond is unsuited to poor-vacuum applications is that the presence of water allows for chemical replacement of hydrogen by hydroxyl groups. This is a slow process but irreversibly drops the electron affinity towards PEA leading to degradation of the electron emission properties. Thus, there are good practical reasons to have a convenient alternative to hydrogen-terminated diamond as an NEA surface. It is also a matter of fundamental interest: there is nothing inherently special about the hydrogen-terminated surface itself and it should not be the only example of a surface termination inducing true NEA. Indeed, the C-H dipoles known to induce the NEA are quite weak and far better examples can be found in theory. Despite this, there is a scant experimental evidence for alternatives. Numerous studies have shown increased electron yield with various alkali oxides, alkali halides and transition metals but none have been shown conclusively to induce true NEA.

Recently, on the basis of theoretical predictions [15] we investigated lithium deposition on the oxygenated diamond surface [16] and showed the existence of a true NEA following a thermal activation step. There is hope that this and similar systems will form the basis of a new class of alternative true NEA surfaces for diamond. In this article we seek to bring together the background, theoretical and experimental work done to date on lithiated diamond.

Kane O'Donnell received his PhD in Physics from the University of Newcastle (Australia) in 2010. His first postdoctoral position was with the University of Bristol (UK) where he worked in the Bristol Centre for Nanoscience and Quantum Information and the School of Chemistry until 2012. From 2012 to 2014 he worked at the Australian Synchrotron (Melbourne) as a postdoctoral fellow before moving to Curtin University (Perth) in early 2014 where he is presently a postdoctoral research fellow in the Department of Imaging and Applied Physics. His research interests are focused on semiconductor surfaces, particularly the interaction of atoms and molecules with diamond and silicon.

2 Brief review of alternative approaches to NEA The first investigations of NEA in the context of electron emission predate the discovery of the true NEA state of diamond and were carried out on Si [17, 18] and GaAs [19, 20] surfaces. Thus, the original "NEA" surfaces actually exhibited what is known as an effective NEA, where strong downwards band-bending at the surface allows the bulk CBM to be above the vacuum level despite the electron affinity being positive. This case is illustrated along with those of PEA and true NEA in Fig. 1. It is possible to induce effective NEA (e-NEA) on numerous semiconductors including silicon and gallium arsenide by heavy p-doping followed by a reduction in the work function using deposited CsO overlayers. The heavy p-doping pins the chemical potential in the bulk relative to the VBM such that there is strong band-bending towards the surface. The CsO overlayer reduces the combined work function of the substrate/overlayer system through the formation of a surface dipole (omitted in Fig. 1b) that can be several eV in magnitude [18]. Effective NEA surfaces formed through this process are used extensively for photocathodes and spin-polarized electron sources. Nevertheless, the electron affinity of these surfaces is positive. As noted by Yater [21], the secondary electron emission spectra of effective and true NEA surfaces is similar in shape (if not magnitude) and consequently it is not sufficient to deduce NEA solely from secondary electron spectra.

In the absence of known values for the work function and E_F–E_{VBM} (Fig. 1), the presence of NEA can be revealed through total photoyield spectroscopy (TPYS) where a characteristic onset is seen when the photon energy reaches the band gap of diamond. Unfortunately, no TPYS studies exist for diamond surfaces other than that of the hydrogen-terminated (111) and (100) surfaces (e.g. Refs [10] and [14]) with the exception of the recent work on lithiated diamond. Nevertheless, there is good reason to suspect that there is at least one class of diamond surface that yields true NEA, those involving caesium oxide coatings. These are fabricated by analogy with the previously mentioned Si and GaAs emitters on the basis that charge transfer within Cs-O complexes impart a significant surface dipole. Theoretical impetus for diamond was provided by Pickett [22] who carried out a study on a 0.5 ML coverage of Cs on oxygen-terminated diamond. The calculations suggest that true NEA should be achieved at this coverage. More important is the fundamental difference between the surface structure of

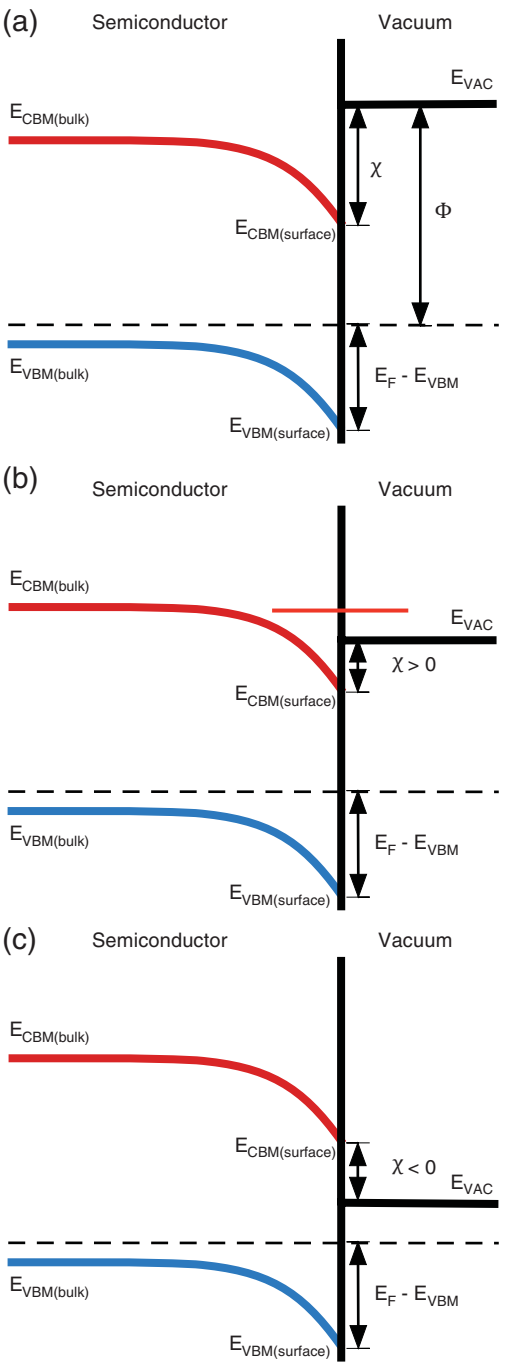

Figure 1 Schematic band diagrams illustrating the relationship between the conduction band minimum (CBM), valence band maximum (VBM) and Fermi level for a semiconductor surface with (a) positive electron affinity (PEA), (b) effective negative electron affinity (eNEA), and (c) true negative electron affinity (NEA).

diamond versus other semiconductors: diamond does not support a native oxide: rather, oxygen atomically terminates diamond. As such, the approach to depositing CsO on diamond is not the same as used for Si and GaAs. In those semiconductors, Cs is first deposited to the appropriate coverage, followed by O_2 exposure. This procedure is known not to have any significant effect on electron emission from diamond [23] beyond the improvement induced solely from the presence of Cs. Instead, the diamond can be first oxygenated and then Cs deposited. This is the approach taken by Loh [24]. We note that on silicon, for example, the oxygenation cannot be carried out first because it results in the formation of an amorphous oxide. An early observation by Goldstein [18] suggests that amorphous overlayers of CsO are not sufficient to induce (effective) NEA on Si – crystalline layers are required. The surface dipole of the silicon itself is not altered but the overlayer possesses a strong dipole moment of its own [25]. Intuitively, one expects that in the case of diamond it will be much harder to produce a crystalline overlayer of Cs due to the very large difference between the atomic size of Cs and C/O.

Pickett argued that the large atomic size of Cs was an advantage because it results in a large Cs-O distance on the surface and consequently a larger dipole moment [22]. However, this is at the cost of a relatively weak binding energy computed as only 1.34 eV/Cs atom. The weak binding energy is no doubt responsible for the poor thermal stability of CsO-coated diamond compared to hydrogen-terminated diamond. For example, Loh et. al., reports thermal stability only up to 500 °C for the CsO-terminated diamond [24] compared to the value of 740 °C reported by Kataoka et al. [6] for the hydrogen terminated surface. It was because of the low binding energy of Cs that we originally investigated the smaller alkali metals.

We digress briefly to discuss other work function-lowering coatings for diamond. The alkali-halides have been studied experimentally by Wong, et al. Both LiF [26] and RbF [27] reduce the work function of diamond as measured using photoemission. However, the deduction that these surfaces exhibit a NEA relies on the assumption that E_F-E_{VBM} is not significantly changed between the clean surface and the deposited surfaces, an unlikely situation for a wide band gap semiconductor such as diamond. Without accompanying TYPS measurements it is not clear whether true NEA is achieved. Furthermore, RbF was found to degrade rapidly upon electron irradiation due to the loss of fluorine whilst the thickness of LiF required to significantly reduce the work function of diamond is such that it is effectively a bulk LiF film. Lithium fluoride has been predicted computationally to actually possess a NEA itself [28] but is a true insulator with no reasonable prospect of doping. These materials are therefore not really suitable alternatives to hydrogen-terminated diamond.

The adsorption of transition metals on diamond has been reported in the context of electron emission in several publications. Elements studied include Cu [29], Co [29–31], Ni [32], Ti [33] and Zr [29, 31]. The results reported are somewhat varied, with photoemission indicating some degree of NEA induced by thin films of Zr, Co, and Ni, although it is not clear whether any of these are true NEA or only effective NEA. Metal–diamond contacts have proven to be a complex subject and the lack of atomic-resolution scanning tunnelling microscopy images for the early stages

of metal film growth makes it difficult to make definitive statements about the character of such interfaces. At this stage, it seems that transition metal adsorbates may hold some promise for electron emission, but more work needs to be done to understand the structural and electronic nature of the underlying metal–diamond interfaces. The existing theoretical work is somewhat confusing on this point. For example, small changes in structure at idealized metal–diamond interfaces are known to lead to abnormally large changes in the predicted Schottky barrier height [34, 35].

Finally, we turn to the alkali metals other than caesium as deposited on diamond. In terms of experimental work not including our own work on lithium, only K-adsorbed diamond has been reported [36–38], except for a field emission study reporting on Cs, K, and Na overlayers in addition to numerous treatments [39]. Electron emission in the latter study was found to be improved by alkali adsorption as would be expected. Photoemission results on these surfaces are not otherwise forthcoming. Petrick and Bennedorf found that the sticking coefficient of K atoms on oxygen-terminated diamond is far higher than that on hydrogen-terminated diamond and essentially unity [36]. This is the expected result and raises the prospect of producing strong chemical bonding for alkalis on diamond surfaces. The key, then, is to find some balance between strong chemical bonding to the substrate and a large dipole moment.

Nie et al. studied the adsorption of Na, K, and Rb on the clean C(100) surface using density functional theory [40, 41]. All these adsorbates are relatively large compared to the diamond lattice constant and unsurprisingly they bond relatively weakly with adsorption energies typically 0.5–1.5 eV depending on coverage and adsorption site. Alkali bonding to diamond-like semiconductors relies on a relatively weak alkali-substrate bond and consequently is not ideal. It is known from studies of alkali adsorption on Si(100) [42] and Ge(100) [43] that there exist significant size effects such that the larger the alkali atom, the weaker the substrate bonding. This is clearly worst in the case of diamond where the lattice constant is considerably smaller than that of the alkalis with the exception of lithium.

3 Lithiated diamond

3.1 Early motivation It is perhaps unsurprising that our initial work on lithiating diamond was wholly unrelated to surfaces and instead focussed on lithium doping for the purpose of producing n-type diamond. The successful doping of diamond by lithium has been long desired because the predicted donor level of interstitial lithium in diamond is approximately 0.1 eV [44], far superior than the best experimentally-demonstrated donor (phosphorus, $E_D = 0.6$ eV). To this end, a lithium in-diffusion method based on a mixture of lithium hydride and nanodiamond was developed with the hope of producing doped, highly conducting nanodiamond powder for thermionic emission applications. LiH and nanodiamond material (300–500 nm HPHT powder, Microdiamant AG) were mixed together in varying

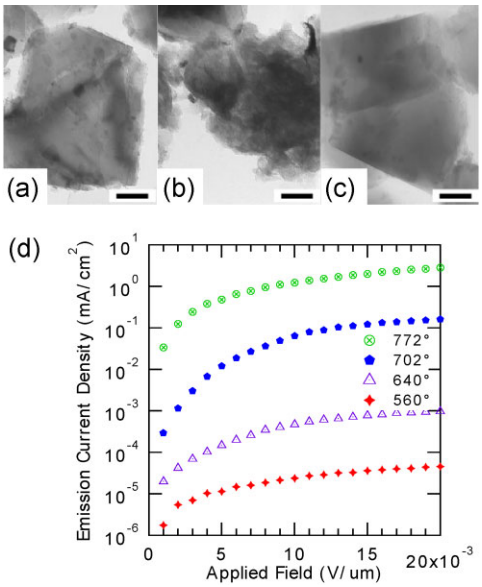

Figure 2 TEM images of nanodiamond material (a) as received, (b) after lithiation treatment prior to water washing, (c) after acid washing. Scale bar is 100 nm. (d) Thermo-field emission from the lithiated/water washed material as a function of applied field for increasing cathode temperature. Images and data from the thesis of Martin [45].

ratios, typically close to 1:1, and heated under argon to high temperatures up to 900 °C. The resulting material was either used as-is, water washed or acid washed in fuming aqua regia in order to remove the considerable residues of the process observed in TEM (Fig. 2b). SIMS measurements on the powders showed reasonably high quantities of lithium ($\sim 6 \times 10^{18}$ cm^{-3}) in the powder even after acid washing, suggesting either limited in-diffusion or the presence of lithium on the surface of the nanodiamonds. The nanodiamonds were then pressed into small pellets and mounted in a heated tube for thermionic-field emission measurements. An example series of current–voltage curves at increasing temperatures appears in Fig. 2d for the lithiated material after water washing. At the time (~2009), these results were quite encouraging with emission current densities of several mA/cm^2 despite the crude cathode arrangement.

Although the measurements were somewhat scattered due to the difficulty in making reproducible devices, there was an interesting observation: the acid-washed nanodiamonds were found to give a significantly lower effective work function as extracted from a Richardson–Laue–Dushman (RLD) plot. This is counter-intuitive, because acid washing should lead to some degree of oxygen termination and corresponding increased electron affinity and work function. Furthermore, the emission current density from the acid-washed samples was several orders of magnitude lower than that of the raw lithiated material and hence the decreased effective work function may have been circumstantial: RLD work function extraction can be

notoriously sensitive to the emission current. However, it prompted us to consider what sort of surface chemistry results from the lithiation process. This was quite a diverting exercise and quickly morphed into a study of lithium on diamond which, at the time, had not been considered experimentally or theoretically. It is worth pointing out here that the chemistry of the lithium-nanodiamond in-diffusion method remains an unresolved problem.

3.2 Lithium on C(100) We studied lithium adsorption on the C(100) surface using density functional theory for both clean, reconstructed diamond and for the ideal oxygen-terminated C(100)-(1 × 1):O surface [15]. The most relevant structures are shown in Fig. 3 with associated adsorption energies and computed electron affinities in Table 1. To obtain the electron affinity it is necessary to know the position of the CBM. It is well known that DFT typically underestimates band gaps and hence does not give an accurate CBM position. To avoid this problem, the VBM position is first computed using the method of Fall et al. [46] and the CBM position is then deduced by adding the experimental bulk band gap of 5.47 eV. The electron affinity is then obtained by subtracting the computed vacuum level.

For the clean surface the results are essentially as expected: as the smallest alkali, lithium has a far higher binding energy per adsorption than all the other alkali metals, at around 3 eV per atom with some small variation depending on the adsorption site relative to the dimer rows. There is very little evidence of adsorbate-adsorbate interaction, with the binding energies for 0.5 ML coverage very similar to those at 1 ML coverage. This is in contrast to heavier alkali adsorbates, which are simply too big to form a monolayer coverage without significantly reducing the adsorbate binding energy. Here and elsewhere we define 1 monolayer (ML) as one adsorbate per carbon site in the surface unit cell. The lowest energy configuration (Fig. 3c) occurs when the lithium occupies the "pedestal" (HH) and "valley-bridge" (T3) adsorption sites as labelled by Levine [47] and Nie [40].

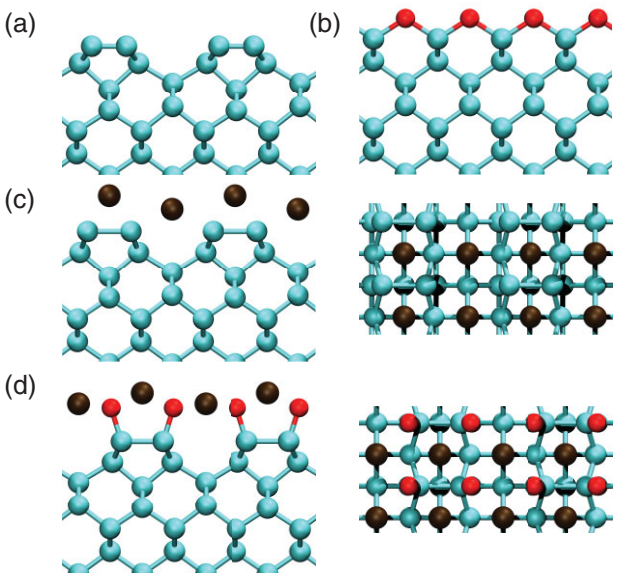

Figure 3 Relaxed structures for lithium adsorption on diamond. (a) View along ⟨011⟩ dimer rows for the clean 2 × 1 surface, (b) the same view for the ether-bridge terminated C(100)-(1 × 1):O surface, (c) views along ⟨011⟩ and ⟨100⟩ for the saturated 1ML C(100)-(2 × 1):Li surface of highest binding energy and (d) the same views for the saturated 1ML C(100)-(2 × 1):LiO surface. Note in (d) the presence of dimers in contrast to the clean oxygen terminated surface in (b). Blue, red, and brown atoms represent carbon, oxygen, and lithium, respectively.

Table 1 Key parameters from DFT simulations for the adsorption of lithium on clean and oxygen-terminated diamond (structures in Fig. 3). From O'Donnell et al. [15].

surface	adsorption energy* (eV per atom)	electron affinity (eV)
C(100)-(2 × 1)	–	0.62
C(100)-(1 × 1):O	8.20	2.63
C(100)-(2 × 1):Li	3.26	−2.70
C(100)-(2 × 1):LiO	4.38	−3.90

*For the C(100)-(2 × 1): LiO surface the adsorption energy is relative to ether-bridge oxygen-terminated diamond, the others are relative to clean diamond.

The effect on the electronic structure of the underlying diamond surface is likewise conventional. For most adsorbate structures of 0.5 ML and 1 ML coverage the computed electron affinity is in the range −2 to −3 eV compared to +0.62 eV for the clean surface. The predicted shift to NEA is caused by significant charge donation to the surface with an overall polar covalent character. The size of the predicted NEA compared to that computed for hydrogen-terminated diamond (−2.2 eV [48]) gives some confidence that the system would exhibit true NEA experimentally.

To summarize, the lithium-on-diamond system is consistent with what is expected based on the absorption of alkalis on silicon and germanium, appropriately accounting for scale. The predicted smaller (negative) electron affinity compared to Cs adsorption as computed by Pickett [22] is offset by the much higher binding energy. Nonetheless, as a practical matter one expects Li-adsorbed C(100) to be highly sensitive to contamination by analogy with the K-adsorbed C(100) [36].

Lithium adsorption on the oxygenated surface (Fig. 3d) is a much more interesting case. The Li–O bond is far stronger than that of the polar covalent bonding between lithium and the clean diamond surface. At stoichiometric saturation coverage, each carbon surface site is bonded to a single O atom that itself is further bonded to a Li atom. On that basis, the C(100)-(2 × 1): LiO surface is the lithium analogue of the hydroxylated C(100)-(2 × 1): OH surface [49]. In both cases the underlying diamond structure possesses the dimer reconstruction of the clean surface albeit

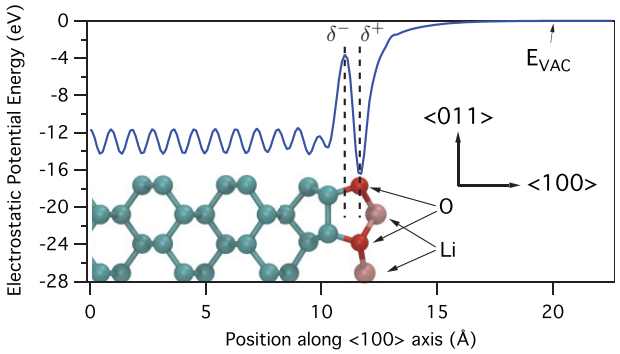

Figure 4 Plane-averaged electrostatic potential showing the surface dipole generated by the Li–O system on the C(100)-(2 × 1):LiO surface. Notice the negative side of the dipole is centred between the C–O bonds on the surface and not on the O sites themselves. From O'Donnell et al. [16].

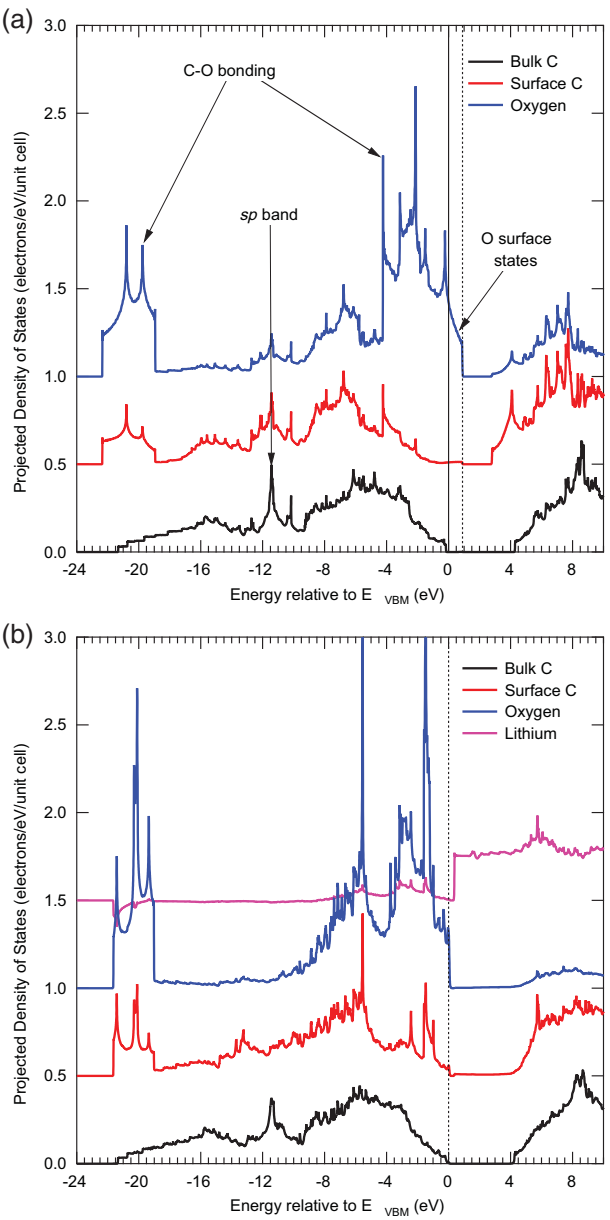

Figure 5 Atom-projected density of states (PDOS) for (a) the C(100)-(1 × 1):O ether-bridged surface and (b) the C(100)-(2 × 1):LiO surface. The energy scale is set such that the bulk VBM is 0 eV. A vertical dotted line indicates the energy position of the highest occupied state.

with somewhat longer dimer C–C bond lengths. However, in the case of lithium there is a further degree of crystallinity where each lithium atom interacts equally with the surrounding four oxygen atoms and vice-versa (Fig. 3d). The lithium atoms are tightly incorporated into the oxygen-terminated surface structure.

Intuitively, one would expect that such a structure would not suit our purpose of generating a large surface dipole: it is in total contrast to traditional systems using large alkalis (e.g. Cs) where the Cs atoms protrude a long way from the surface and the resulting atomic separation is key to the dipole moment. In actual fact, the LiO surface dipole is very large. This can be seen in the plane-averaged electrostatic potential along the (100) axis as shown in Fig. 4. The key observation here is that the dipole is not atom-centred on the Li–O sites. Thus, the fact that the Li–O displacement vector is almost in the plane of the surface is irrelevant as it is not the vector relevant to calculation of the dipole moment.

Electronically, we explain the formation of this dipole through the formation of a delocalized charge enhancement at the dimer-oxygen interface. The presence of the Li atoms lowers the energy of the oxygen lone-pair states such that they overlap considerably with the high-lying sp^2 bonding states of the dimer. This leads to a further degree of hybridization and delocalization of charge associated with the oxygen. This negative side of the dipole is countered by the positive Li atoms (Fig. 4). The lowering of electronic states can be observed in the projected density of states (Fig. 5). For the oxygen-terminated surface there are occupied surface states extending approximately 0.9 eV above the VBM whereas on the lithiated surface these states are not present and their bonding character instead is shifted to lower energies overlapping with the surface carbon valence states.

The consequence of the electronic changes upon lithium adsorption is a strong dipole leading to a change in the VBM position of −4.52 eV relative to the clean (2 × 1) surface and a predicted electron affinity of −3.90 eV. As with the solely Li-deposited surface the size of the predicted NEA is comparable to that computed for hydrogen-terminated diamond (indeed, it is significantly larger in this case). At the same time, the LiO-terminated surface should be considerably more stable than Li adsorbed on clean C(100) not just because the adsorption energy is higher per atom but because the lithium is already fully oxidized and consequently attacks by typical contaminant species (e.g., H_2O, CO, and CO_2) are far less likely to occur.

In addition, it should also be the case that the Li surface is the most chemically stable on oxygen-terminated diamond with 1 ML Li coverage. Our calculations bear this out– adding additional Li atoms above 1 ML coverage yields a very low binding energy for the extra atoms [50]. This is ideal because it makes the prospect of actually fabricating such a surface much easier: excess lithium should be less stable with respect to, for example, thermal annealing therefore facilitating easy removal of the excess.

3.3 Lithium on C(111) The (100)-oriented surface is no doubt the most important for single-crystal applications and polycrystalline material when the diamond is grown on a substrate that encourages (100)-oriented growth. However, for nanodiamonds the (111)-oriented surface may be equally important [51, 52].

We have studied lithium adsorption on the (111)-oriented diamond surface, both clean and oxygen-terminated. The clean C(111)-(2 × 1) surface is generally believed to reconstruct into π-bonded Pandey chains in common with other (111) semiconductor surfaces [53, 54]. Lithium adsorption yields a weak adsorption energy, of about 1.2–1.5 eV, and minimal sensitivity to the adsorption site. Density functional theory calculations suggest that the nominally preferred site is the bridge position on top of the Pandey chains at low coverage up to 0.5 ML but at higher coverage the preferred adsorption structure shifts to a displaced on-top site (Fig. 6a). The computed electron affinity is approximately −0.81 eV which makes it hard to predict with confidence whether lithiated C(111) should possess true NEA experimentally.

In the oxygen-terminated C(111) case the situation is complicated by the fact that there are two distinct forms of oxygen adsorption that appear to interconvert with coverage [55]. We first focus on the maximum coverage of 1 ML of oxygen which is in the form of carbonyl bonding and breaks the Pandey chains (Fig. 6b). At this oxygen coverage, each lithium on the lithium-saturated surface is threefold-coordinated to oxygen (Fig. 6c). The lithium atoms are not as well-incorporated into the surface structure as for oxygen terminated C(100) (Fig. 3d). The resulting adsorption energy is comparable to the C(100):O surface at 3.54 eV per lithium atom, however the computed electron affinity is much smaller (−1.13 eV) and consequently it is not clear that 1 ML Li on oxygen-terminated C(111) will possess negative electron affinity. We note that the optimal 1 ML lithium-adsorbed surface in this case has carbon chains along the surface that have the appearance of Pandey chains (though without the characteristic π-bonding), with the oxygen atoms no longer double-bonded to surface carbons.

As a practical matter, the difficulty with C(111) surfaces for lithiation is that sub-saturation coverages (of either lithium or oxygen) give improved properties for both adsorption energy and VBM shift, in contrast to the C(100) surface where ideal LiO-termination is optimal. For example, for the 1 ML oxygen-terminated C(111) surface (Fig. 6b), 0.5 ML lithium (Fig. 7a) yields both higher adsorption energies and much larger shift in the VBM position than the associated 1 ML lithium-adsorbed surface (see Table 2). Sub-stoichiometric surfaces are potentially undesirable here because they are chemically unsaturated and therefore may be unstable outside ultra-high vacuum. A

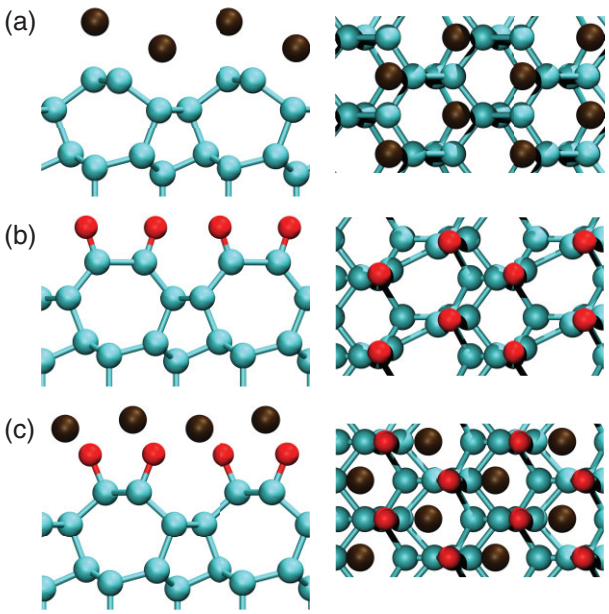

Figure 6 Optimized structures for (a) 1 ML Li adsorption on clean, Pandey-reconstructed C(111), (b) the reference full-coverage oxygen-terminated C(111) surface and (c) 1 ML Li adsorption on the oxygen-terminated C(111) surface.

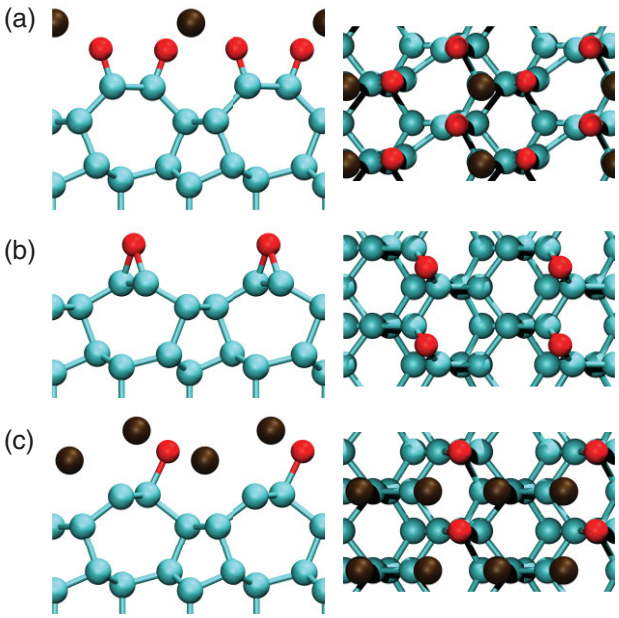

Figure 7 Structural views of (a) the lowest-energy 0.5 ML Li adsorption state on 1 ML oxygen-terminated C(111), (b) epoxy-bonded 0.5 ML oxygen-terminated C(111) and (c) 1 ML Li adsorption on 0.5 ML oxygen-terminated C(111).

Table 2 Key parameters from DFT simulations for the adsorption of lithium on clean and oxygen-terminated diamond. From the thesis of Martin [45].

surface	adsorption energy* (eV per atom)	electron affinity (eV)
C(111)-(2 × 1):Li	1.50	−0.81
C(111)-(2 × 1):LiO	3.54	−1.13
C(111)-(2 × 1):LiO (0.5 ML lithium)	4.37	−3.97
C(111)-(2 × 1):LiO (0.5 ML oxygen)	2.69	−3.10

*For the C(111)-(2 × 1): Li surface the adsorption energy is relative to clean, Pandey-reconstructed C(111). The others are relative to the relevant underlying oxygen-terminated surface.

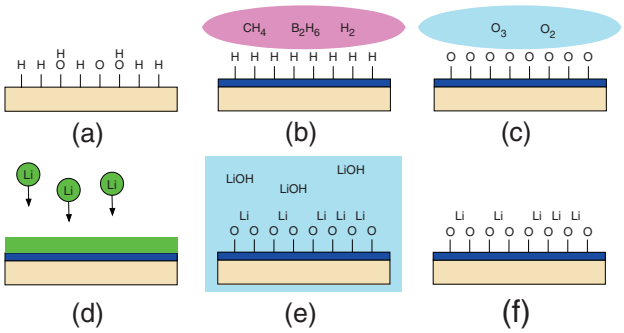

Figure 8 Thick film process for fabrication of lithiated diamond. (a) Intrinsic <100>substrates are prepared with (b) boron-doped epitaxial overlayers. (c) The surface is oxygen-terminated, typically by ozone exposure, then (d) lithium is thermally deposited to a thickness of 50–200 nm. (e) Immersion at room temperature in DI water removes most of the lithium products, leaving only (f) small traces of lithium remaining. From Martin et al. [57].

similar situation arises for lower coverages of oxygen. Up to 0.5 ML of oxygen, it is found that the stable oxygen-adsorption structure is an epoxy form that preserves the carbon chains on the surface [24, 55] (Fig. 7b). In this case, 1 ML lithium (Fig. 7c) yields an acceptable adsorption energy (2.69 eV) and electron affinity (−3.10 eV), both superior to the stoichiometric surface. Since it is known that alkali metals enhance clean diamond reactivity towards oxygen [36] it may be necessary to use the traditional yo-yo method of first adsorbing the lithium followed by oxygen exposure in order to lithiate the C(111) surface effectively.

The key observation of the theoretical work on lithium adsorption is that the combination of lithium and oxygen is critical to satisfying the goals of high adsorption energy and a sufficiently large surface dipole leading to negative electron affinity. The most satisfactory combination is LiO-termination of the C(100)-(2 × 1) surface. We have examined two approaches to fabricating such a system starting from oxygen-terminated diamond: a thick-film approach starting from a large quantity of lithium and reducing it, and a thin-film approach where a low-rate dispenser source is used to incrementally add lithium.

4 Experimental work

4.1 Thick-film process The thick-film process [56, 57] is illustrated schematically in Fig. 8. Substrates used for surface science experiments such as photoemission require a conductive surface and hence we first grow epitaxial overlayers of boron-doped diamond on (100) single crystal substrates (Element 6). The samples are then oxygen-terminated. We have used three methods for oxygen-termination: plasma, ozone, and acid-washing. There are small spectroscopic differences in the C 1s core level spectra for these different techniques, suggesting slightly different bonding, but the coverage is similar. For the thick film process, the first lithiation step is to deposit a thick (50–200 nm) film of Li metal from a thermal effusion cell under moderate vacuum. The resulting film will react in air to form products such as LiOH, Li_2O, and Li_2CO_3. We rely on these products to offer some degree of protection to the lithium–diamond interface for the brief atmospheric exposure required.

Lithium compounds are typically soluble or react with water to form lithium hydroxide, itself soluble. Therefore, immersion of the lithium-deposited substrate into DI water removes the vast majority of lithium. Indeed, one would expect that only lithium sufficiently strongly bonded to the oxygen-terminated diamond surface would remain. The average coordination number for a lithium ion in solution is found from simulations to be in the range 4–6 (with a mean of 4.8) [58] and hence in the case of lithium bonded to the surface there may be an enhanced barrier to solvation that works in favour of the process. High-quality de-ionised water is required in this process because clearly if lithium can 'stick' to the surface in the water, there is scope for contamination from other alkali and alkaline earth metal ions that may already be present in the water. It is straightforward to show that any residual contamination in DI water has little effect on electron emission relative to the lithium: Fig. 9 shows an SEM image of a sample masked during lithium evaporation so that the Li film was only grown in the lower left corner of the film. After immersion in DI (Milli-Q) water, the secondary electron yield of the lithium-deposited half of the sample is much higher than that of the clean half, demonstrating that any contaminants remaining in Milli-Q DI water contribute very little to the modification of electron emission properties.

Photoemission can be used to verify the presence of lithium after the water immersion. Figure 10 shows the Li 1s core level spectra acquired using a lab-based XPS system ($h\nu = 1486.6$ eV, unmonochromated source, pass energy 50 eV) for the thick Li film after deposition and after water immersion for both oxygen-terminated and hydrogen-terminated diamond as a control substrate. Water immersion is seen to remove essentially all the lithium on the hydrogen-terminated substrate. Some lithium remains on the oxygen-terminated substrate after immersion, and importantly, it is observed to have a different chemical state to that of the as-deposited film. The core level spectrum for the thick lithium

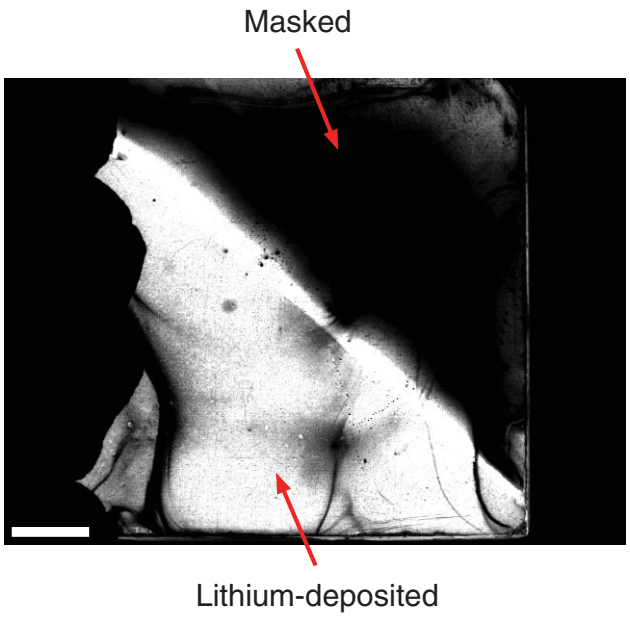

Figure 9 SEM image of a C(100) substrate first oxygen-terminated then masked prior to undergoing steps d–f from the thick-film process (Fig. 8). The whole crystal was immersed in DI water to remove the thick lithium film. The dark irregular boundary on the left edge of the crystal is carbon dag. Scale bar (lower left) is 500 μm.

film is dominated by a peak at 57.6 eV, probably due to lithium carbonate given the very large core level shift, with a smaller component at 55.5 eV likely to be LiOH/Li_2O [59]. The water-immersed sample is in contrast dominated by a broad feature centred around 55.6 eV. Since the water-immersed sample is dried in air prior to measurement, it has a similar probability to form carbonate from hydroxide as the thick film. The diminished relative presence of lithium carbonate is evidence that the lithium is involved in diamond surface chemistry and not simply in the form of a lithium compound.

Ultraviolet photoelectron spectroscopy (UPS) shows that surfaces prepared by the thick-film lithiation process have a similar signature in electron emission to that of hydrogen-terminated diamond. Figure 11 shows the He I UPS spectra for oxygen-terminated diamond, hydrogen-terminated diamond and lithiated diamond. The spectra are approximately normalized to the valence band feature near −8 eV. Both the hydrogen-terminated and lithiated spectra show characteristic high secondary electron yield at around −16 eV associated with the emission of thermal electrons from the conduction band minimum, suggestive of negative electron affinity. The exact energy position of the conduction band minimum is difficult to determine accurately from UPS spectra alone because it is necessary to know the energy difference between the Fermi level and the valence band maximum at the surface (E_F–E_{VBM}, see Fig. 1) which is not easily measured without synchrotron photoemission measurements. However, it is clear that lithiated diamond has

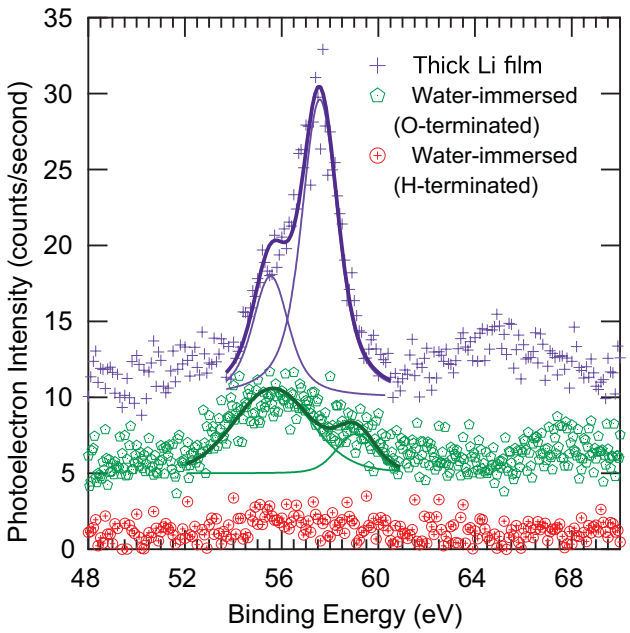

Figure 10 Li 1s core level spectra for the as-deposited thick metal film and water-immersed surfaces for both oxygen-and hydrogen-terminated diamond. Lithium only remains after water immersion in the case of oxygen-terminated diamond. Spectra are offset in intensity for clarity.

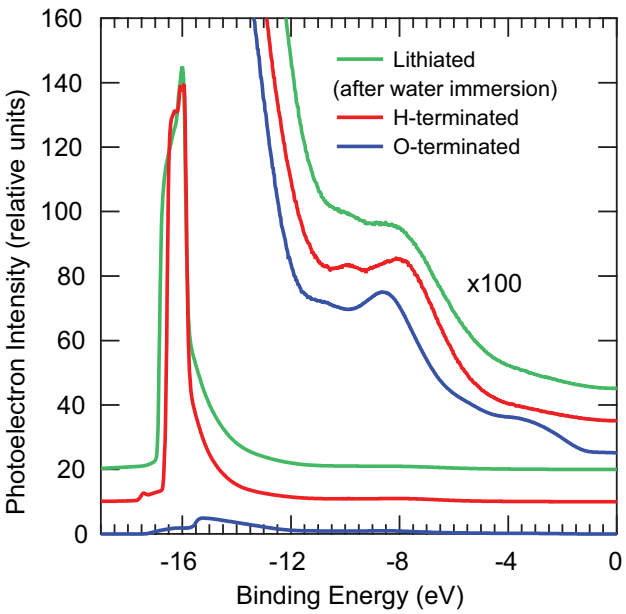

Figure 11 Ultraviolet photoelectron spectra of oxygen-terminated, hydrogen-terminated, and lithiated diamond generated using He I (21.22 eV) light and with a sample bias of −9 V applied to overcome the work function of the analyser and to ensure good collection of low kinetic energy electrons.

electron emission characteristics more similar to those of a known NEA surface (hydrogen-terminated diamond) than those of a known PEA surface (oxygen-terminated diamond). We briefly note here that the large "CBM peak" in our spectra is not a single dominant peak but possesses some structure to higher binding energies. We have submitted a manuscript on this point very recently where we examine both hydrogen-terminated and lithiated diamond in detail using synchrotron radiation. We believe the structures originate in general from phonon scattering, with the details only fully resolved when the analyser pass energy is comparable to the mean optical phonon energy in diamond (~155 meV [60]).

The primary issue with the thick-film process is that reproducibility is not ideal. As can be observed in the SEM image of a typical surface (Fig. 9), there is considerable spatial variation in electron emission, partially due to residues left over from drying during the water immersion process. The parameter space for optimising the process is quite large. Given the ease with which good electron emitters can be produced with this method it is worthwhile examining the process further, however the poor reproducibility in the resulting surface makes fundamental investigation of the underlying surface chemistry quite difficult. Therefore, we have also examined lithiated diamond via a thin-film process starting from a well-characterized oxygen-terminated surface.

4.2 Thin-film process The starting point for the thin-film process [16] is identical to that of the thick-film process with intrinsic <100>-oriented single crystals with boron-doped epitaxial overlayers grown on top, followed by an oxygen-termination step. Figure 12 shows the sequence in full. In our studies of the thin-film process we typically used oxygen plasma (50 W, 5 min, with no deliberate substrate heating) to terminate the surface, though acid-washing has also been found to work. The particular acid wash used is

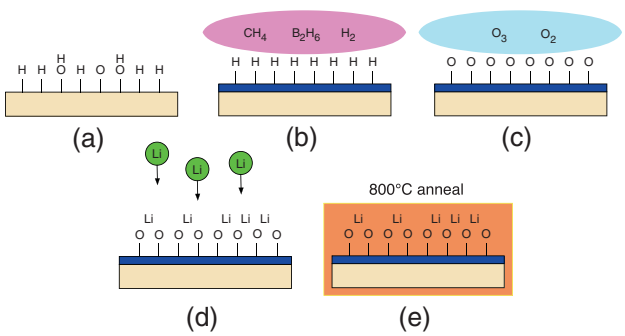

Figure 12 Schematic diagram for the thin-film process. (a) Starting with intrinsic diamond, (b) a boron-doped conductive overlayer is grown on top and (c) the surface is oxygen-terminated by exposure to an oxygen plasma (alternatively an acid wash). (d) Under UHV conditions, a lithium dispenser source is used to deposit submonolayer coverages of Li and (e) the surface is "activated" through thermal annealing.

30 min in boiling concentrated sulphuric acid (200–300 °C) followed by the addition of 1 M potassium nitrate to give fuming nitric acid. A further boil for 30 min and a water rinse completes the wash. After oxygen-termination, samples are introduced into an ultra-high-vacuum (UHV) environment and remain there for the rest of the processing and analysis. A light anneal (300 °C) is used to remove weakly adsorbed contaminants and then a lithium dispenser source (SAES) is used to deposit small quantities of Li giving only submonolayer coverages.

We measured the low kinetic energy electron spectra of secondary electrons using 150 eV photons at the Soft X-ray beamline of the Australian Synchrotron [61]. Experimentally, it is found that the deposition of lithium in this fashion has little effect on the electron yield and leads to only small changes in the work function. Instead, it is found that a thermal annealing process is required to "activate" the surface. This is illustrated best by the series of low kinetic energy spectra acquired as a function of annealing temperature (Fig. 13a). After a 400 °C anneal for 15 min there is a sudden decrease in the work function by almost 1 eV. After 600 °C, a very sharp emission feature appears at the low-energy cutoff with peak emission almost ten times that of the plain lithium-deposited surface. A further anneal at 800 °C reveals a low-kinetic energy peak 55 × higher than the reference. Further annealing at 800 °C led to a maximum peak intensity of approximately 100 × the reference and 20 × the total integrated yield. This is all with a tiny quantity of lithium estimated at (0.40 ± 0.05) Å, which if evenly distributed would be approximately 0.2 monolayers. Further deposition and annealing gives peak intensities of over 200 × the reference with the total integrated yield increased by a factor of 40. This series is shown graphically in Fig. 13b.

We interpret these large changes in electron emission as a move from positive electron affinity to negative electron affinity as a consequence of annealing. Indeed, in our measurements it is possible to see all three states – PEA, *effective* NEA and *true* NEA, with the effective NEA occurring after the 600 °C anneal. The very sharp feature observed in Fig. 13a has the character of a vacuum-level cutoff, as one would expect if the vacuum level lies between the bulk and surface conduction band minima due to band-bending (see Fig. 1b). Nevertheless, once the vacuum level has moved below the CBM there is no longer a clear vacuum level cutoff and consequently one cannot measure the work function. Therefore, to establish unequivocally the presence of true negative electron affinity, it is necessary use a technique such as total photoelectron yield spectroscopy (TPYS). There is a well-established signature for NEA in TPYS spectra consisting of a sudden increase in yield when the photon energy reaches the bandgap energy [10–12, 62–64]. The increase in yield arises from electron emission from the conduction band minimum. Our TPYS experiments were carried out at Institut für Technische Physik, Universität Erlangen, Germany and necessitated sending a prepared (thermally activated) sample in an argon-backfilled

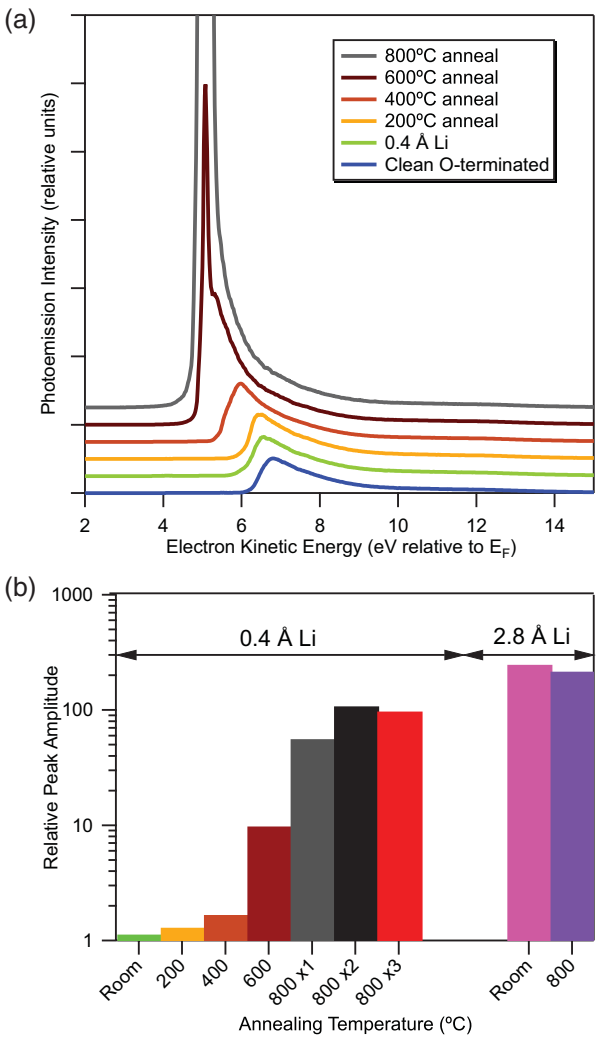

Figure 13 (a) Low kinetic energy spectra acquired at 150 eV photon energy for the initially clean oxygen-terminated diamond surface followed by 0.4 Å lithium deposition and annealing in steps of 200 °C. (b) The peak intensity for each annealing step relative to the as-deposited surface. Colours match those in part (a). The final two entries show the further lithium deposition and annealing. Note log scale on the *y*-axis. From O'Donnell et al. [16].

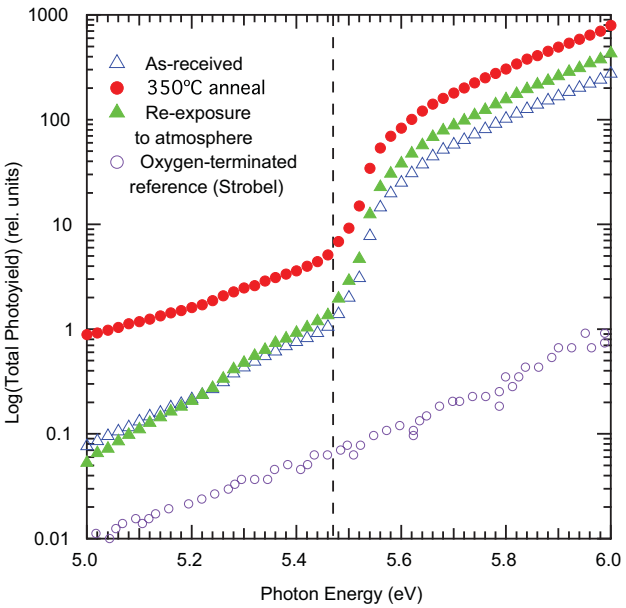

Figure 14 Total photoelectron yield spectra for the as-received diamond sample (open triangles), after a light anneal (closed circles) and after re-exposure to atmosphere (closed triangles). All show the characteristic step in yield once the photon energy increases past the band gap energy (dashed vertical line). A reference spectrum from a sample with positive electron affinity – oxygen-terminated diamond – is shown for comparison.

container. Consequently, the sample had some air exposure prior to introduction into the TPYS system. Nevertheless, the as-received sample shows the expected NEA signature even without annealing (Fig. 14). A light anneal improves the electron yield slightly, likely due to the removal of atmospheric adsorbates, but nowhere near the orders of magnitude change observed for hydrogen-terminated diamond when exposed to air. By re-exposing to air it is found that the TPYS spectrum returns to that of the as-received sample, demonstrating that indeed it is simply weakly-adsorbed atmospheric adsorbates that cause the slight reduction in yield.

The relative insensitivity of the lithiated surface to air-exposure is a major benefit for devices that rely on electron emission because it permits a poorer vacuum within the device. The reason for the stability must be related to a lack of surface transfer doping in air. A lithiated and activated sample is found to have no measurable surface conductivity when exposed to atmosphere [16]. However, more recent measurements of surface transfer doping (as yet unpublished) using $C_{60}F_{48}$ as an electron acceptor show the same spectroscopic signatures of surface transfer doping as those of hydrogen-terminated diamond [65]. That is, both charged and uncharged dopant molecules can be observed on the lithiated surface using core-level photoemission spectroscopy, and a shift in the value of E_F–E_{VBM} is measured as a function of dopant coverage. These indicate that surface transfer doping on lithiated diamond is wholly conventional despite the lack of measurable conductivity. Consequently, we hypothesize that the observed air stability results from the fact that the initial band-bending on lithiated diamond is already considerable, typically (0.7 ± 0.2) eV. To generate a hole accumulation layer at the surface, it is necessary to dope sufficiently such that the Fermi level crosses the valence band at the surface, i.e. E_F–E_{VBM} becomes negative. In the case of lithiated diamond, this requires a very large shift in E_F–E_{VBM} that has not presently been achieved. However, there is some reason to believe that it is not impossible. The *theoretical* ideal lithiated surface – C(100)-(2×1):LiO – should not have significant band bending at the surface because occupied surface states do not intrude into the band gap (see Fig. 5). It follows that optimization of the

fabrication process may lead to lithiated diamond surfaces with a similar utility as hydrogen-terminated diamond in terms of surface transfer doping. This would be very useful because the lithiated surface is unlikely to suffer from long-term hydroxylation outside a UHV environment.

5 Future work There are two primary limitations that need addressing in order to optimise the lithiation process, both using thin-film or thick-film methods. The first is that oxygen-termination methods are still poorly understood. Nominally oxygen-terminated <100> diamond surfaces exhibit a (1×1) low energy electron diffraction (LEED) pattern as would be expected for ideal ether-bridge oxygen-termination. However, it could also reflect the bulk periodicity due to surface disorder. Indeed, the LEED patterns for oxygen-terminated diamond are often quite diffuse compared to the sharp 2×1 patterns observed for carefully prepared hydrogen-terminated <100> diamond [66]. This suggests oxygen-terminated diamond surfaces in general have smaller <100> terraces and a larger fraction of step edges, detrimental to the formation of crystalline overlayers of the sort shown in Figure 3. Developments in methods for 'soft' oxygen-termination of <100> diamond that preserve the relatively large terraces of properly prepared hydrogen-terminated diamond would be expected to improve the effects of lithiation considerably. Atomically-flat oxygen termination has been achieved on <111> surfaces both from the growth phase [67, 68] and using wet chemistry [69] but similar methods are yet to be demonstrated on <100> surfaces.

The second limitation is that the need for thermal activation belies a surface process that is not yet fully understood. In particular, it appears necessary to thermally activate the surface when using the thin-film process to achieve the characteristic increase in electron yield, yet the thick-film process gives a surface with high electron yield immediately. There is some evidence to suggest that a diamond prepared through the thick-film process has improved yield properties upon annealing but it is difficult to distinguish the improvements as due to lithium surface chemistry rather than simply the removal of surface contamination and residues from the water immersion process. Certainly the improvements bear no resemblance to the $200\times$ improvement in electron yield obtained with the thin film process. We have recently completed a theoretical study to be written up shortly which considers the chemistry of small numbers of lithium atoms on an oxygen-terminated surface. The calculations suggest that isolated lithium atoms on a large oxygen-terminated slab do not generate the large surface dipole seen for high-coverage lithium in small unit-cell calculations. This is not simply due to the low coverage but because several Li atoms are required to be next to each other in order to lift the ether-bridge structure of the underlying oxygen-termination, allowing the formation of (2×1) unit cells featuring a C–C dimer. As identified earlier, the negative charge of the lithium-oxygen dipole system is centred on the dimers and hence is critical to surface dipole formation. These observations may explain why thermal annealing is required for low coverages of lithium. An experimental study at crossover coverages is certainly required in this area.

In addition to understanding and optimising the lithiation process, there are both fundamental and applied questions of interest yet to be investigated. For example, what chemical interactions are likely to be significant for lithiated diamond, particularly involving polar solvents? The ability of lithiated diamond to act as a source of solvated electrons in the fashion of Zhu and Hamers [7] depends critically on whether lithium remains bound to the surface in the long term. There is also the question of extending the lithium-oxygen system to other elements. For example, we have recently completed a series of simulations to be submitted shortly, in order to connect the well-established work on the heavier alkalis to those of lithium, magnesium and sodium. We find that Mg adsorption creates a similar electronic structure as Li adsorption, as expected given the diagonal chemical relationship between the two elements. Sodium, however, is found to be at the transition point between the "normal" atom-centred dipoles seen for the heavier alkali metals and the primarily delocalized dipoles generated by Li and Mg. Experimental investigation of this series is highly desirable. Finally, there is a need to incorporate lithiated diamond into device architectures: photocathodes, current amplifiers, vacuum electronics, thermionic converters and so on, in order to investigate whether it really does stand as a useful alternative to hydrogen-terminated diamond. At the very least, it gives an opportunity to investigate the phenomenon of NEA in more detail by inducing the same electron emission properties but with a totally different surface chemistry.

6 Conclusions In this article, we have tried to present a summary of the work done on negative electron affinity lithiated diamond. Starting with oxygen-terminated diamond, Li deposition and a thermal activation leads to a $200\times$ increase in secondary electron yield intensity. Lithiated diamond does not suffer from band-bending induced emission suppression and consequently can withstand exposure to atmosphere without significant degradation in electron yield. Two fabrication processes have been discussed in detail and we show that although they produce similar electron emission properties there are still sufficiently different characteristics between the two that more work is required to bridge the gap between the thick-film and thin-film regimes. In particular, the question remains why thermal activation is necessary for the thin film process and why it appears less critical for the thick-film process. We have also reviewed our published theoretical work underpinning our experimental efforts, with a particular focus on the distinct "delocalized" dipole generated by the Li-O system on the C(100) surface. We believe this dipole mechanism explains how the small Li ion can generate a significant surface dipole even without protruding a significant distance from the surface. By

exploring the parameter space and optimizing the lithiation process, we expect lithiated diamond will form a useful negative electron affinity diamond surface for electron emission applications.

Acknowledgements The authors would like to thank Paul May (University of Bristol) and Qi-Hui Wu (Quanzhou Normal University) for growing the boron-doped diamond films used in the studies presented here. We acknowledge the support and expertise of Bruce Cowie of the Soft X-Ray beamline at the Australian Synchrotron for the photoemission and low kinetic energy electron emission measurements. KOD thanks Neil Allan (University of Bristol) for many useful discussions regarding computational studies of adsorption on surfaces. This work was supported by the Multi-modal Australian ScienceS Imaging and Visualisation Environment (MASSIVE) (www.massive.org.au). Part of this work was carried out using the computational facilities of the Advanced Computing Research Centre, University of Bristol - http://www.bris.ac.uk/acrc/.

References

[1] J. S. Foord, C. H. Lau, M. Hiramatsu, A. Bennett, and R. B. Jackman, Diam. Relat. Mater. **11**, 437 (2002).
[2] J. S. Foord, C. H. Lau, and M. Hiramatsu, Carbon **43**, 2106 (2005).
[3] A. S. Tremsin and O. H. W. Siegmund, Diam. Relat. Mater. **14**, 48 (2005).
[4] X. Chang, Q. Wu, I. Ben-Zvi, A. Burrill, J. Kewisch, T. Rao, J. Smedley, E. Wang, E. Muller, R. Busby, and D. Dimitrov, Phys. Rev. Lett. **105**, 164801 (2010).
[5] D. Takeuchi, S. Koizumi, T. Makino, H. Kato, M. Ogura, H. Ohashi, H. Okushi, and S. Yamasaki, Phys. Status Solidi A **210**, 1961 (2013).
[6] M. Kataoka, C. Zhu, F. A. M. Koeck, and R. J. Nemanich, Diam. Relat. Mater. **19**, 110 (2010).
[7] D. Zhu, L. Zhang, R. E. Ruther, and R. J. Hamers, Nature Mater. **12**, 836 (2013).
[8] F. Himpsel, J. Knapp, J. Van Vechten, and D. Eastman, Phys. Rev. B **20**, 624 (1979).
[9] B. B. Pate, B. Waclawski, P. Stefan, C. Binns, T. Ohta, M. Hecht, P. Jupiter, M. Shek, D. Pierce, and N. Swanson, Physica B+C **117**, 783 (1983).
[10] C. Bandis and B. B. Pate, Phys. Rev. Lett. **74**, 777 (1995).
[11] C. Bandis and B. B. Pate, Phys. Rev. B **52**, 12056 (1995).
[12] C. Bandis and B. B. Pate, Surf. Sci. **350**, 315 (1996).
[13] F. Maier, M. Riedel, B. Mantel, J. Ristein, and L. Ley, Phys. Rev. Lett. **85**, 3472 (2000).
[14] D. Takeuchi, M. Riedel, J. Ristein, and L. Ley, Phys. Rev. B **68**, 041304 (2003).
[15] K. M. O'Donnell, T. Martin, N. A. Fox, and D. Cherns, Phys. Rev. B **82**, 115303 (2010).
[16] K. M. O'Donnell, M. T. Edmonds, J. Ristein, A. Tadich, L. Thomsen, Q. H. Wu, C. I. Pakes, and L. Ley, Adv. Funct. Mater. **23**, 5608 (2013).
[17] R. U. Martinelli, Appl. Phys. Lett. **16**, 261 (1970).
[18] B. Goldstein, Surf. Sci **35**, 227 (1973).
[19] J. J. Scheer and J. Van Laar, Solid State Commun. **3**, 189 (1965).
[20] B. Goldstein, Surf. Sci **47**, 143 (1975).
[21] J. E. Yater and A. Shih, Appl. Surf. Sci. **143**, 219 (1999).
[22] W. E. Pickett, Phys. Rev. Lett. **73**, 1664 (1994).
[23] O. Küttel, O. Gröning, E. Schaller, L. Diederich, P. Gröning, and L. Schalpabach, Diam. Relat. Mater. **5**, 807 (1996).
[24] K. Loh, X. Xie, S. Yang, J. Pan, and P. Wu, Diam. Relat. Mater. **11**, 1379 (2002).
[25] B. F. Williams, and J. J. Tietjen, Proc. IEEE **59**, 1489 (1971).
[26] K. W. Wong, Y. Wang, K. Lee, and R. Kwok, Diam. Relat. Mater. **8**, 1885 (1999).
[27] K. Wong, Y. Wang, S. Lee, and R. Kwok, Appl. Surf. Sci. **140**, 144 (1999).
[28] A. B. Kunz, T. Miyakawa, and S. Oyama, Phys. Status Solidi B **34**, 581 (1969).
[29] P. Baumann and R. J. Nemanich, Diam. Relat. Mater. **7**, 612 (1998).
[30] P. Baumann and R. J. Nemanich, Appl. Surf. Sci. **104**, 267 (1996).
[31] P. Baumann and R. J. Nemanich, J. Appl. Phys. **83**, 2072 (1998).
[32] J. Van der Weide and R. J. Nemanich, Phys. Rev. B **49**, 13629 (1994).
[33] J. Van der Weide and R. J. Nemanich, J.Vacuum Sci. Technol. B **10**, 1940 (1992).
[34] W. E. Pickett and S. C. Erwin, Phys. Rev. B **41**, 9756 (1990).
[35] W. E. Pickett, M. R. Pederson, K. A. Jackson, and S. C. Erwin, Mater. Sci. Eng. B **14**, 87 (1992).
[36] S. Petrick and C. Benndorf, Diam. Relat. Mater. **10**, 519 (2001).
[37] M. Hossain, T. Kubo, T. Aruga, N. Takagi, T. Tsuno, N. Fujimori, and M. Nishijima, Diam. Relat. Mater. **9**, 162 (2000).
[38] M. Hossain, T. Miki, H. Okuyama, T. Aruga, T. Tsuno, N. Fujimori, T. Ando, and M. Nishijima, Diam. Relat. Mater. **2049**, 10. (2001).
[39] N. A. Fox, W. Wang, K. Hallam, P. May, J. Stone, and M. Ashfold, Diam. Relat. Mater. **7**, 671 (1998).
[40] J. L. Nie, H. Y. Xiao, X. T. Zu, and F. Gao, Chem. Phys. **326**, 308 (2006).
[41] J. L. Nie, H. Y. Xiao, X. T. Zu, and F. Gao, Physica B **383**, 219 (2006).
[42] L. S. O. Johansson and B. Reihl, Surf. Sci. **287**, 524 (1993).
[43] H. Y. Xiao, X. T. Zu, Y. F. Zhang, and F. Gao, Chem. Phys. Lett. **417**, 6 (2006).
[44] S. Kajihara, A. Antonelli, J. Bernholc, and R. Car, Phys. Rev. Lett. **66**, 2010 (1991).
[45] T. L. Martin, Lithium Oxygen Termination as a Negative Electron Affinity Surface on Diamond: A Computational and Photoemission Study (University of Bristol, 2012).
[46] C. Fall, N. Binggeli, and A. Baldereschi, J. Phys.: Condens. Matter **11**, 2689 (1999).
[47] J. D. Levine, Surf. Sci. **34**, 90 (1973).
[48] J. Van der Weide, Z. Zhang, P. Baumann, M. Wensell, J. Bernholc, and R. J. Nemanich, Phys. Rev. B **50**, 5803 (1994).
[49] S. Sque, R. Jones, and P. Briddon, Phys. Rev. B **73**, 085313 (2006).
[50] K. M. O'Donnell, T. L. Martin, N. A. Fox, and D. Cherns, MRS Proc. 1282, mrsf10 (2011).
[51] L. Lai, and A. S. Barnard, J. Mater. Chem. **22**, 16774 (2012).
[52] A. S. Barnard, S. P. Russo, and I. K. Snook, Diam. Relat. Mater. **12**, 1867 (2003).
[53] K. C. Pandey, Phys. Rev. Lett. **49**, 223 (1982).
[54] K. C. Pandey, Phys. Rev. B **25**, 4338 (1982).
[55] K. P. Loh, X. N. Xie, S. W. Yang, and J. C. Zheng, J. Phys. Chem. B **106**, 5230 (2002).

[56] N. Fox, T. L. Martin, and K. M. O'Donnell, US 8,617,651 B2 (31 December 2013).
[57] T. L. Martin, K. M. O'Donnell, H. Shiozawa, C. E. Giusca, N. A. Fox, S. R. P. Silva, and D. Cherns, MRS Proc. 1282, mrsf10 2011.
[58] P. Maye and M. Mezei, J. Mol. Struc.-Theochem. **362**, 317 (1996).
[59] J. Hoenigman and R. Keil, Appl. Surf. Sci. **18**, 207 (1984).
[60] A. Bosak and M. Krisch, Phys. Rev. B **72**, 224305 (2005).
[61] B. C. C. Cowie, A. Tadich, and L. Thomsen, AIP Conf. Proc. **1234**, 307 (2010).
[62] D. Takeuchi, C. E. Nebel, and S. Yamasaki, Phys. Status Solidi A **203**, 3100 (2006).
[63] D. Takeuchi, C. E. Nebel, and S. Yamasaki, J. Appl. Phys. **99**, 086102 (2006).
[64] D. Takeuchi, S. G. Ri, H. Kato, C. E. Nebel, and S. Yamasaki, Diam. Relat. Mater. **15**, 698 (2006).
[65] M. T. Edmonds, M. Wanke, A. Tadich, H. M. Vulling, K. J. Rietwyk, P. L. Sharp, C. B. Stark, Y. Smets, A. Schenk, Q. H. Wu, L. Ley, and C. I. Pakes, J. Chem. Phys. **136**, 124701 (2012).
[66] P. Pehrsson and T. Mercer, Surf. Sci **460**, 49 (2000).
[67] N. Tokuda, H. Umezawa, S.-G. Ri, M. Ogura, K. Yamabe, H. Okushi, and S. Yamasaki, Diam. Relat. Mater. **17**, 1051 (2008).
[68] N. Tokuda, H. Umezawa, K. Yamabe, H. Okushi, and S. Yamasaki, Diam. Relat. Mater. **19**, 288 (2010).
[69] N. Tokuda, D. Takeuchi, S.-G. Ri, H. Umezawa, K. Yamabe, H. Okushi, and S. Yamasaki, Diam. Relat. Mater. **18**, 213 (2009).

